Front. Phys., 2012, 7(3): 360–365
DOI 10.1007/s11467-011-0193-0

RESEARCH ARTICLE

Mechanical properties of bcc Fe–Cr alloys by first-principles simulations

Xiao-qing Li (李晓庆)[1,2], **Ji-jun Zhao** (赵纪军)[1,2,†], **Jing-cheng Xu** (徐京城)[1,2]

[1] *Key Laboratory of Materials Modification by Laser, Electron, and Ion Beams, Dalian University of Technology, Ministry of Education, Dalian 116024, China*

[2] *College of Advanced Science and Technology, Dalian University of Technology, Dalian 116024, China*

E-mails: [†] *zhaojj@dlut.edu.cn*

Received May 16, 2011; accepted June 10, 2011

The effect of chromium content on the fundamental mechanical properties of Fe–Cr alloys has been studied by first-principles calculations. Within a random solid solution model, the lattice constants and the elastic constants of ferromagnetic bcc $Fe_{1-x}Cr_x$ ($0 \leqslant x \leqslant 0.156$) alloys were calculated for different compositions. With addition of Cr content, the lattice parameters of Fe–Cr alloys are larger than that of pure Fe solid, and the corresponding Young's modulus and shear modulus rise non-monotonically with the increasing Cr content. All alloys (except 9.4 at% Cr) exhibit less ductile behavior compared with pure bcc Fe. For the $Fe_{1-x}Cr_x$ ($0 \leqslant x \leqslant 0.156$) alloys, the average magnetic moment per atom decreases linearly with the increasing Cr concentration.

Keywords Fe–Cr alloys, mechanical properties, lattice constant, magnetic moment

PACS numbers 88.30.R-, 88.30.rd

1 Introduction

Reduced activation ferritic/martensitic steels (RAFM steels) based on the body centered cubic (bcc) Fe–Cr alloys (7–12 wt% Cr) with some trace elements (W, V, Si, C) are considered as the primary structural materials in the first wall and blanket structure of future fusion reactor owing to their attractive properties [1–8], such as the excellent resistance to swelling and embrittlement under irradiation [6], low neutron activation level [8], and good thermal and mechanical properties [7]. Considerable efforts have been devoted to finding optimal compositions of the Fe-based alloys that can endure the extreme environments of fusion reactors.

At present, several countries have developed their own receipt of RAFM steels, such as EUROFER9 [1, 5], F82H [1, 9], JLF-1 [10], 9Cr–2WVTa [11], and CLAM [12]. Experimental studies reveal that addition of Cr into pure Fe or steels can significantly affect the mechanical properties of Fe–Cr alloys and ferritic/martensitic steels as well as their behavior under irradiation [8, 13–17]. For example, Klueh *et al.* studied the strengths of three RAFM steels (Fe–2.25Cr–2WVTa, Fe–2.6Cr–2WVTa, and Fe–9Cr–2WVTa), and they found that the strengths of the 2.6Cr steel is slightly below those of the 2.25Cr and 9Cr steels [14]. Neutron irradiated ferritic steels show clear dependence of tensile properties on the Cr content [8]. In the low temperature range, steels with 7% to 9% of Cr exhibit less irradiation hardening with regard to those with 2.25Cr and 12Cr steels.

However, the co-existence of multi-elements in RAFM steels makes the characterization of their mechanical properties complicated. To understand the fundamental mechanical properties and the irradiation effect of the RAFM steels better, binary bcc Fe–Cr alloys as model systems of the multi-component steels become the main subject of research [13, 15, 16, 18–20]. Porollo *et al.* studied the tensile properties of Fe–Cr alloys (with 0, 2, 6, 12 and 18 wt% Cr) under the neutron irradiated condition at the room temperature. They found that both ultimate and yield strengths of these alloys increase monotonically with the increasing Cr content [19]. Speich *et al.* [20] measured the elastic constants of Fe–1.5Cr, Fe–5Cr, Fe–6Cr, and Fe–10Cr alloys and found that the Cr content reduced Poisson's ratio (ν) as well as the ratio of bulk modulus and shear modulus (B/G).

To our knowledge, most experimental efforts of the binary Fe–Cr alloys have been devoted to the understanding of the effect of chromium content on the irradiation

behaviors; however, little attention was paid to the effect of Cr concentration on the fundamental mechanical properties, such as elastic properties and ductile/brittle behaviors, which may serve as a guidance for further optimizing the composition of RAFM steels. In addition, the magnetic constraint of plasma is an essential requirement for fusion reaction. Since iron-based solid of bcc phase is ferromagnetic, it may affect the magnetism field configuration inside the reactor and consequently disturb the plasma stability. Hence, it is important to investigate the magnetic properties of the Fe–Cr alloy as a function of Cr concentration. In this paper, within a random solid solution model we calculated the equilibrium lattice constants and elastic constants of $Fe_{1-x}Cr_x$ ($0 \leqslant x \leqslant 0.156$) alloys as the functions of the chemical composition, and evaluated their ductile/brittle properties. The magnetic moments of the binary Fe–Cr solids with different Cr contents were also computed and discussed.

2 Model and computational methods

A random solid solution model was used for the $Fe_{1-x}Cr_x$ alloys ($0 \leqslant x \leqslant 0.156$). The model was described by a 128-atom cubic supercell built from 4×4×4 bcc unit cell. First, a Fe supercell with 128 atoms was created. Then, part of Fe atoms were randomly substituted by the Cr atoms to obtain various alloys with different Cr contents, that is, Fe (Fe_{128}), Fe–3.1%Cr ($Fe_{124}Cr_4$), Fe–5.5%Cr ($Fe_{121}Cr_7$), Fe–7.8%Cr ($Fe_{118}Cr_{10}$), Fe–9.4%Cr ($Fe_{116}Cr_{12}$), Fe–11.7%Cr ($Fe_{113}Cr_{15}$), Fe–14.1%Cr ($Fe_{110}Cr_{18}$) and Fe–15.6%Cr ($Fe_{108}Cr_{20}$). A representative structure ($Fe_{116}Cr_{12}$) is shown in Fig. 1. For each composition, ten random configurations were generated. After the first-principles optimization, the one with the lowest energy was selected for further study on the mechanical properties.

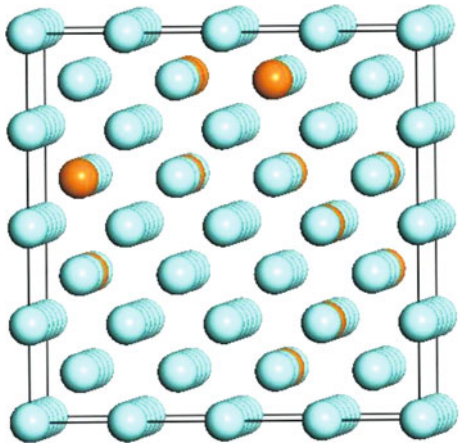

Fig. 1 128-atom supercells of bcc $Fe_{116}Cr_{12}$ alloys (Fe–9.4Cr) within a random solid solution model.

First-principles calculations were performed using density functional theory (DFT) and projector-augmented wave (PAW) method [21, 22] as implemented in the Vienna Ab-initio Simulation Package (VASP) [23]. We adopted the generalized gradient approximation (GGA) of the Perdew and Wang (PW91) functional to describe the exchange–correlation interaction [24]. The Brillouin zone was sampled by a 2×2×2 $\boldsymbol{k}$ grid generated by Monkhorst–Pack scheme. The cutoff energy was chosen as 350 eV. Further increasing cutoff energy or $\boldsymbol{k}$ grid has little effect on the computational results.

Within the framework of continuum elasticity theory [25, 26], the three independent elastic constants C_{11}, C_{12}, and C_{44} for the present cubic systems can be obtained by applying appropriate homogeneous strains. In practice, the elastic constants (C_{11}, C_{12}, and C_{44}) were determined by applying a set of three strain tensors ε below:

$$\begin{pmatrix} \xi & 0 & 0 \\ 0 & 0 & 0 \\ 0 & 0 & 0 \end{pmatrix} \quad \begin{pmatrix} \xi & 0 & 0 \\ 0 & \xi & 0 \\ 0 & 0 & \xi \end{pmatrix} \quad \begin{pmatrix} \xi & 0 & 0 \\ 0 & 0 & \xi \\ 0 & \xi & 0 \end{pmatrix} \tag{1}$$

and fitting the elastic energy as a function of the small strain parameters ξ [26].

Afterwards, the bulk modulus (B), (isotropic) shear modulus (G), (isotropic) Young's modulus (E), Poisson's ratio (ν) and Cauchy pressure (C') of the cubic Fe–Cr crystals can be calculated from C_{11}, C_{12}, and C_{44} via the following relations:

$$B = (C_{11} + 2C_{12})/3 \tag{2}$$

$$G = (3C_{44} + C_{11} - C_{12})/5 \tag{3}$$

$$E = 9BG/(3B + G) \tag{4}$$

$$\nu = -1 + E/(2G) \tag{5}$$

$$C' = (C_{12} - C_{44})/2 \tag{6}$$

3 Results and discussion

3.1 Lattice constant and elastic constants of ferromagnetic bcc crystal of Fe

In order to assess the reliability of our computational methods, Table 1 and Table 2 list equilibrium lattice parameter, single-crystal elastic constants, and polycrystalline (isotropic) elastic moduli of the ferromagnetic bcc Fe from our DFT calculations along with those from previous first-principles calculations [27, 28] and experiments [29]. It can be seen that the present lattice parameter deviates the experimental value by about –1.6%. This may be ascribed to the GGA–PW91 functional used in this work, which is known to underestimate the equilibrium volume of magnetic 3d metals [30, 31]. Similar underestimation of lattice parameter was found in previous DFT calculations with ultrasoft pseudopotentials (PP) [27] and full-potential linear muffin-tin orbitals (FP–LMTO) method [28].

Table 1 Lattice constant (a), elastic constants (C_{ij}), and average magnetic moment per atom (m_s) for ferromagnetic solid of bcc Fe. Previous experimental and theoretical values are also presented for comparison.

	a/Å	C_{11}/GPa	C_{12}/GPa	C_{44}/GPa	$m_s/(\mu_B/\text{atom})$
This work	2.823	280.0	151.5	119.8	2.19
PP[a]	2.830	289.0	118.0	115.0	–
FP–LMTO[b]	2.810	297.0	148.0	123.0	–
Expt.[c]	2.870	243.1	138.1	121.9	–
Expt.[d]	2.870	–	–	–	2.22

[a]Ref. [27], [b]Ref. [28], [c]Ref. [29], [d]Ref. [37].

Table 2 Young's modulus (E), Poisson's ratio (ν), bulk modulus (B), shear modulus (G), B/G ratio, and Cauchy pressure C' of ferromagnetic solid of bcc Fe. Previous experimental and theoretical values are also presented for comparison.

	E/GPa	ν	B/GPa	G/GPa	B/G	C'/GPa
This work	250.7	0.286	194.0	97.6	1.98	15.85
PP[a]	256.2	0.260	175.0	102.0	1.72	1.50
FP–LMTO[b]	263.9	0.280	201.0	103.0	1.95	18.65
Expt.[c]	239.1	0.270	173.1	94.1	1.84	8.05

[a]Ref. [27], [b]Ref. [28], [c]Ref. [29].

Compared with the experimental elastic constants [29], the present calculations have yielded fairly accurate values of C_{12} and C_{44}, but have overestimated C_{11} by about 15%. In addition, the B/G ratio, shear modulus (G), Young's modulus (E) and Poisson's ratio (ν) from our calculations agree well with experimental values, with deviations from experiments of about 7%, 4%, 5% and 6%, respectively. Overall, our present method is able to describe the mechanical properties of Fe–Cr alloys with reasonable accuracy.

3.2 Lattice constants and elastic constants of Fe–Cr alloys

We now discuss the effect of Cr content x on the structural and elastic properties of the bcc $Fe_{1-x}Cr_x$ alloys. Figure 2 compares the calculated lattice parameters for the Fe–Cr alloys with the experiment values [32] and previous calculations with EMTO method [33]. Similar to the case of pure iron solid, both the present and previous DFT calculations underestimate the lattice constants by about 0.02–0.03 Å in experiments. Meanwhile, our calculated results show similar trend as the previous EMTO data [33], which are much closer to the experimental ones. In general, the EMTO method does not allow ions to relax, and it requires some empirical parameters in screening interaction. On the contrary, no empirical parameter was used in our calculation and all ions were also allowed to fully relax. This is the advantage of our calculation. Nonetheless, here we wanted to focus on the variation trend of lattice constant as a function of Cr atomic content. Besides obtaining a similar trend as those from EMTO calculations, we got the lattice parameters which differ from EMTO calculations by only about 0.01 Å within the range of Cr concentrations investigated. With the addition of Cr content, the lattice parameters of Fe–Cr alloys are larger than that of pure Fe solid. This can be partially explained by the larger lattice constant of bcc antiferromagnetic solid of chromium (2.842 Å) as opposed to that of bcc pure iron (2.823 Å) from our DFT calculations. Furthermore, both the present calculations and Zhang's previous work [33] predicted a non-linear relationship between the lattice parameter and the Cr content, whereas experiments exhibit a nearly linear relationship. Generally, the agreement between our calculations and previous experimental and theoretical results is satisfactory.

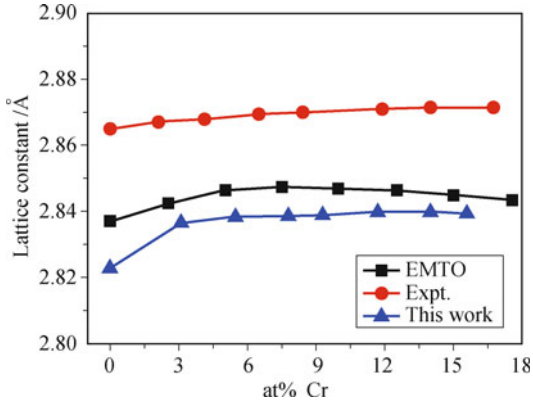

Fig. 2 Lattice parameter of ferromagnetic bcc Fe–Cr alloys as a function of Cr concentration. Previous experimental [32] and theoretical (EMTO) [33] data are also plotted for comparison.

For each Cr concentration x, the elastic constants and other mechanical parameters of ferromagnetic $Fe_{1-x}Cr_x$ alloys with bcc phase were calculated at the equilibrium lattice parameter $a(x)$. The calculated elastic constants are shown in Table 3 and plotted in Fig. 3 as a function of x. Similar to the previous finding by Zhang and coworkers [33], C_{11}, C_{12} and C_{44} have local minima around 5.5 at% Cr. These minimal elastic constants are lower than the corresponding values of pure Fe by 6%, 10.6%, and 15%, respectively. This implies the presence of anomalous electronic transitions around this concentration. Recently, Korzhavyi *et al.* [34] reported a so-called

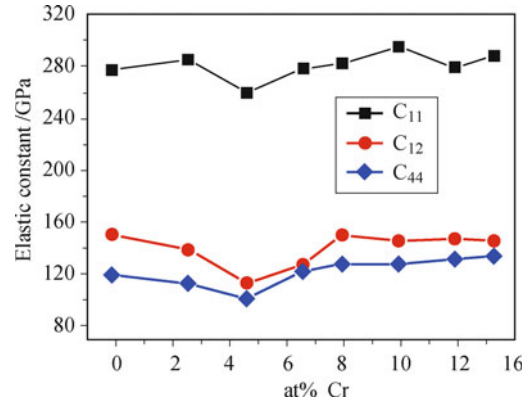

Fig. 3 Elastic constants of ferromagnetic bcc Fe–Cr alloys as functions of Cr concentration.

Table 3 Lattice constants (a), elastic constants (C_{ij}), and average magnetic moment per atom (m_s) for the ferromagnetic bcc solid of $Fe_{1-x}Cr_x$ alloys ($0 \leqslant x \leqslant 0.156$).

x	a/Å	C_{11}/GPa	C_{12}/GPa	C_{44}/GPa	$\frac{C_{11}-C_{12}}{2}$/GPa	m_s /(μ_B/atom)
0	2.8231	280.0	151.5	119.8	64.3	2.190
0.031	2.8368	288.0	139.5	113.1	74.3	2.143
0.055	2.8386	262.0	113.5	101.3	74.3	2.059
0.078	2.8387	281.0	128.5	122.2	76.5	1.958
0.094	2.8390	285.0	151.0	117.3	67.0	1.891
0.117	2.8400	298.0	146.5	128.3	75.8	1.812
0.141	2.8399	282.0	148.0	132.3	67.0	1.750
0.156	2.8396	291.0	146.5	134.5	72.3	1.701

electron topological transition of the Fermi surface in the majority-spin channel in Fe–Cr alloys with about 7 at% Cr. Hence, we suggest that the observed anomalous trend of the elastic parameters around 5.5 at% Cr may be related to such topological transition.

The theoretical polycrystalline elastic parameters for ferromagnetic bcc $Fe_{1-x}Cr_x$ alloys are listed in Table 4 and plotted as a function of Cr concentration x in Fig. 4. The experimental values [20] are also shown for comparison.

Table 4 Young's modulus (E), Poisson's ratio (ν), bulk modulus (B), shear modulus (G), B/G ratio, and Cauchy pressure C' for the ferromagnetic bcc solid of $Fe_{1-x}Cr_x$ alloys ($0 \leqslant x \leqslant 0.156$).

x	E/GPa	ν	B/GPa	G/GPa	B/G	C'/GPa
0	250.7	0.286	194.0	97.6	1.980	15.86
0.031	249.6	0.279	189.0	97.5	1.938	13.20
0.055	229.0	0.266	163.0	90.5	1.800	6.13
0.078	259.6	0.256	180.0	103.1	1.75	3.00
0.094	250.1	0.287	195.7	97.2	2.014	16.90
0.117	272.0	0.27	197.0	107.3	1.840	9.13
0.141	268.7	0.268	192.7	106.0	1.820	7.90
0.156	276.8	0.263	194.7	109.6	1.780	6.00

As shown in Figs. 4(a) and (b), Young's modulus and shear modulus rise non-monotonically with the increasing Cr content. This agrees with the general trend of experimental data [20]. When Cr atomic concentration reaches up to 15.6 at%, the Young's modulus and shear modulus of the Fe–Cr alloys get enhanced by $\sim$ 10.3% and $\sim$ 12.3% relative to those of pure Fe solid, respectively. Our results show similar trends as previous theoretical ones [33], that is, as the Cr atomic concentration reaches up to 15.6 at%, the Young's modulus and shear modulus from our calculations are enhanced by $\sim$ 10.3% and $\sim$ 12.3% relative to those of pure Fe solid, comparable to $\sim$ 9.4% and $\sim$ 12% with the Cr atomic concentration reaching up to 15 at% from previous theoretical calculations [33]. Interestingly, the nonlinear variation of bulk modulus with Cr concentration observed in experiment is well reproduced by our calculations, except for the minor difference in the Cr composition at the minimum (5.5 at% Cr from our calculations and 6 at% measured by experiment).

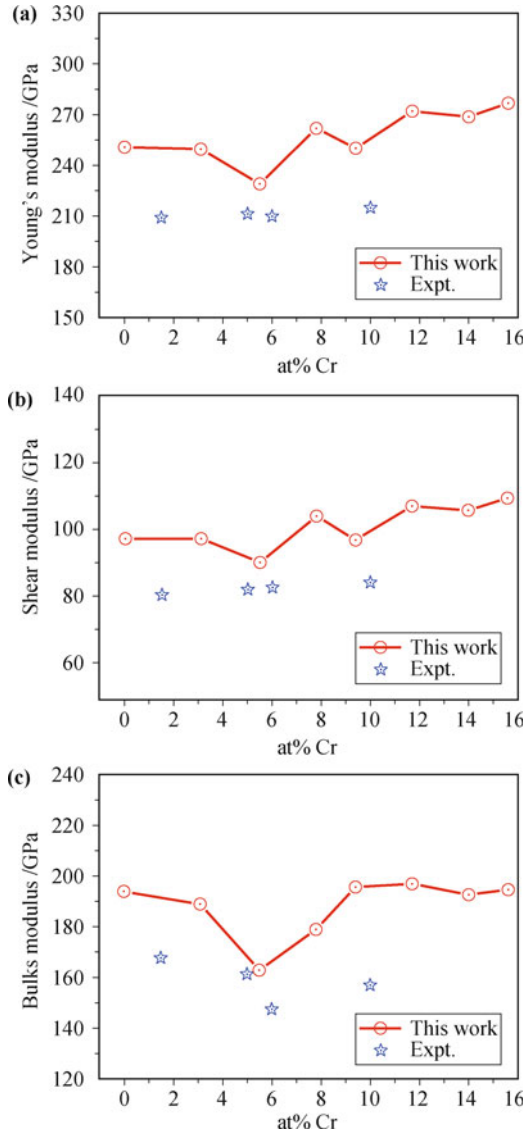

Fig. 4 Young's modulus (E), shear modulus (G) and bulk modulus (B) of ferromagnetic bcc Fe–Cr alloys as functions of Cr concentration. Previous experimental values [20] are also shown for comparison.

We further discuss the ductile/brittle behavior of the $Fe_{1-x}Cr_x$ alloys, which is also crucial for the performance of the structural materials. Previously, Pugh [35] proposed approximate criteria for the ductile/brittle transition by means of the B/G value: A material behaves

in a ductile manner when its B/G ratio is greater than 1.75, otherwise, it is in a brittle regime. In addition, the ductile/brittle behavior of a cubic crystal can also be expressed by its Cauchy pressure: the Cauchy pressure has a positive value if materials exhibit ductility properties, whereas for brittle materials, the Cauchy pressure is negative [36]. As shown in Table 4, the calculated values of B/G are larger than 1.75 for all Fe–Cr alloys, suggesting that all of them exhibit the ductile properties. Figure 5 shows the ratio of the bulk and shear modulus (B/G), Cauchy pressure $(C_{12}–C_{44})/2$, and Poisson's ratio as functions of Cr concentration. One can see that the theoretical values of B/G and Poisson's ratio for ferromagnetic bcc Fe–Cr alloys agree well with the experimental ones. With increasing Cr content, the B/G values gradually decreases and reaches the minimum value of 1.75 at 7.8 at% Cr, and then increases up to a maximum value of 2.0 at 9.4 at% Cr. As is seen, Fe–7.8Cr alloy possesses the least ductile characteristics, while the Fe–9.4Cr alloy presents the strongest ductility among all $Fe_{1-x}Cr_x$ alloys studied ($0 \leqslant x \leqslant 0.156$). This trend matches perfectly the experiment measurement in that there exists a least ductile alloy around 6 at% Cr. Within the present composition range, all alloys except Fe–9.4Cr are less ductile than pure Fe solid. In general, Fe–Cr alloys with low Cr concentration exhibit better ductility. The Cauchy pressure as well as Poisson's ratio from our calculations show similar variation of brittle/ductile behaviors with the Cr concentration.

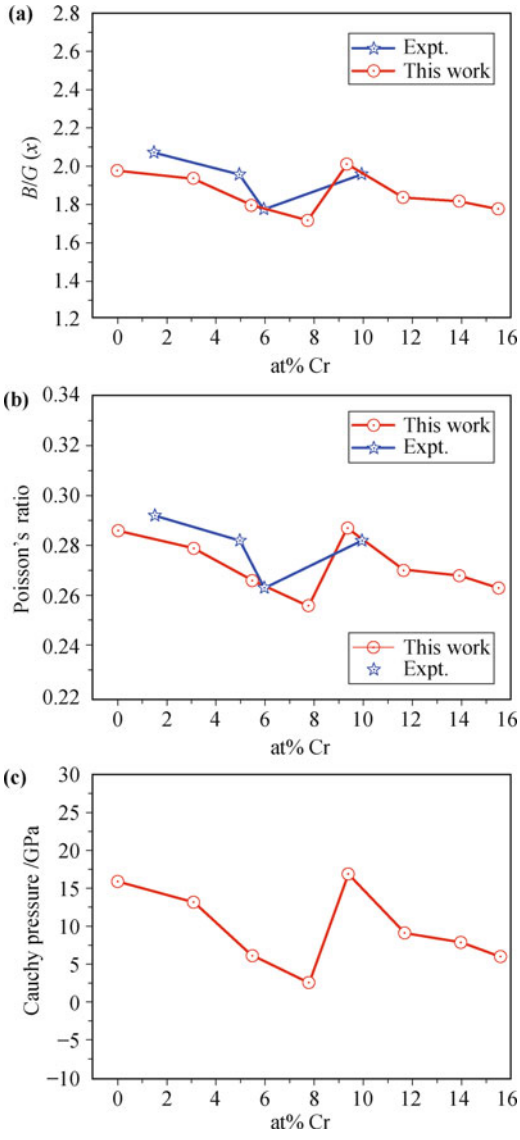

Fig. 5 The B/G ratio, Poisson's ratio and Cauchy pressure of ferromagnetic bcc Fe–Cr alloys as a function of Cr concentration. Previous experimental values (Ref. [20]) are also shown for comparison.

3.3 Magnetic properties of Fe–Cr alloys

Iron and Chromium are constituents of many important magnetic materials. In the form of elementary solid (both with bcc structure), the former is strong ferromagnetic (FM), and the latter is weak incommensurate antiferromagnetic (AF). In the present work, our calculations were performed on random ferromagnetic $Fe_{1-x}Cr_x$ alloys with $0 \leqslant x \leqslant 0.156$ based on the bcc structure. The calculated values of pure Fe solid and Fe–Cr alloys together with the experimental results [37, 38] were listed in Table 1 and Table 3, respectively. For pure Fe solid, the calculated magnetic moment is 2.19 μ_B/atom, in good agreement with the experimental one (2.22 μ_B/atom) [37]. For the Fe–Cr alloys, the average magnetic moments were plotted as a function of Cr concentration and are shown in Fig. 6, in which earlier experimental results are also shown [38]. Clearly, our calculated results present a similar trend as previous experimental ones. The average magnetic moment decreases linearly with an increase in Cr concentration.

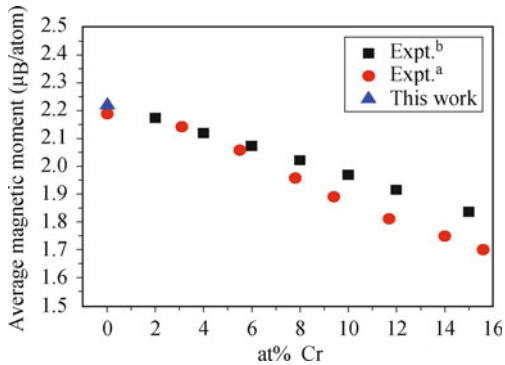

Fig. 6 Average magnetic moments of ferromagnetic bcc Fe–Cr alloys as a function of Cr concentration. Previous experimental values, i.e., Expt.[a] from Ref. [37]. and Expt.[b] from Ref. [38], are also shown for comparison.

To further understand the role of Cr in the magnetism of Fe–Cr alloys, we calculated the local magnetic moments on the Cr and Fe sites in the Fe–11.7Cr alloys. We found that the Cr atom has an average magnetic moment of 1.60 μ_B, which aligns antiferromagnetically with the magnetic moment of Fe sites (2.26 μ_B on av-

erage). This picture is in agreement with the previous finding by Paduani and co-workers [39]. Therefore, the reduction of the average magnetic moment in Fe–Cr alloys ($0 \leqslant x \leqslant 0.156$) due to increasing Cr content may be explained by the antiferromagnetic coupling between the local moments on the Fe and Cr atoms.

4 Conclusions

Within a random solid solution model of bcc solid, first-principles calculations have been performed to investigate the fundamental mechanical and magnetic properties of Fe–Cr alloys as a function of Cr content. According to our theoretical results, with the addition of Cr content, the lattice parameters of Fe–Cr alloys are larger than that of pure Fe solid, and the corresponding Young's modulus and shear modulus rise non-monotonically with the increasing Cr content. For the ductile/brittle properties, all Fe–Cr alloys (except Fe–9.4Cr) appear more brittle than pure Fe. According to the theoretical B/G value and Cauchy pressure, Fe–7.8Cr alloy possesses the strongest brittle characteristics and Fe–9.4Cr alloy presents the top ductility among all $Fe_{1-x}Cr_x$ alloys ($0 \leqslant x \leqslant 0.156$). The average magnetic moment in the $Fe_{1-x}Cr_x$ alloy decreases linearly with the increase of Cr concentration. These theoretical results may provide useful information in designing and optimizing the chemical composition of RAFM steels used for fusion reactor.

Acknowledgements This work was supported by the National Basic Research Program of China (973 Program) (Grant No. 2011GB108007) and the Fundamental Research Funds for the Central Universities of China (Grant No. DUT10ZD211).

References

1. R. L. Klueh, D. S. Gelles, S. Jitsukawa, A. Kimura, G. R. Odette, B. van der Schaaf, and M. Victoria, J. Nucl. Mater., 2002, 307–311: 455
2. A. Kohyama, A. Hishinuma, D. S. Gelles, R. L. Klueh, W. Dietz, and K. Ehrlich, J. Nucl. Mater., 1996, 233–237: 138
3. T. Muroga, M. Gasparotto, and S. J. Zinkle, Fusion Eng. Des., 2002, 61–62: 13
4. A. A. F. Tavassoli, J. Nucl. Mater., 2002, 302(2–3): 73
5. B. van der Schaaf, D. S. Gelles, S. Jitsukawa, A. Kimura, R. L. Klueh, A. Moslang, and G. R. Odette, J. Nucl. Mater., 2000, 283–287: 52
6. F. A. Garner, D. S. Gelles, and F. W. Wiffen, eds., TMS-AIME, 1985
7. A. F. Rowcliffe, J. P. Robertson, R. L. Klueh, K. Shiba, D. J. Alexander, M. L. Grossbeck, and S. Jitsukawa, J. Nucl. Mater., 1998, 258(263): 1275
8. A. Kohyama, Y. Kohno, K. Satoh, and N. Igata, J. Nucl. Mater., 1984, 122(1–3): 619
9. S. Jitsukawa, M. Tamura, B. van der Schaaf, R. L. Klueh, A. Alamo, C. Petersen, M. Schirra, P. Spaetig, G. R. Odette, A. A. Tavassoli, K. Shiba, A. Kohyama, and A. Kimura, J. Nucl. Mater., 2002, 307–311: 179
10. T. Hasegawa, Y. Tomita, and A. Kohyama, J. Nucl. Mater., 1998, 258(263): 1153
11. R. L. Klueh, D. J. Alexander, and M. Rieth, J. Nucl. Mater., 1999, 273(2): 146
12. Q. Y. Huang, J. G. Li, and Y. X. Chen, J. Nucl. Mater., 2004, 329–333: 268
13. V. Krsjak, W. Egger, M. Petriska, and S. Sojak, Probl. Atom. Sci. Tech., 2009, 109.
14. R. L. Klueh, D. J. Alexander, and E. A. Kenik, J. Nucl. Mater., 1995, 227(1–2): 11
15. Z. Lu, R. G. Faulkner, G. Was, and B. D. Wirth, Scripta Materialia, 2008, 58(10): 878
16. M. I. Luppo, C. Bailat, R. Schaublin, and M. Victoria, J. Nucl. Mater., 2000, 283–287: 483
17. R. H. Jones, H. L. Heinisch, and K. A. McCarthy, J. Nucl. Mater., 1999, 271–272: 518
18. D. S. Gelles, J. Nucl. Mater., 1995, 225: 163
19. S. I. Porollo, A. M. Dvoriashin, A. N. Vorobyev, and Y. V. Konobeev, J. Nucl. Mater., 1998, 256(2–3): 247
20. G. R. Speich, A. J. Schwoeble, and W.C. Leslie, Metall. Trans., 1972, 3(8): 2031
21. G. Kresse and D. Joubert, Phys. Rev. B, 1999, 59(3): 1758
22. P. E. Blöchl, Phys. Rev. B, 1994, 50(24): 17953
23. G. Kresse and J. Furthmuller, Phys. Rev. B, 1996, 54(16): 11169
24. J. P. Perdew, J. A. Chevary, S. H. Vosko, K. A. Jackson, M. R. Pederson, D. J. Singh, and C. Fiolhais, Phys. Rev. B, 1992, 46(11): 6671
25. D. C. Wallace, Solid State Physics, New York: Academic, 1970
26. J. J. Zhao, J. M. Winey, and Y. M. Gupta, Phys. Rev. B, 2007, 75(9): 094105
27. L. Vočdlo, G. A. de Wijs, G. Kresse, M. Gillan, and G. D. Price, Faraday Discuss., 1997, 106: 205
28. X. W. Sha and R. E. Cohen, Phys. Rev. B, 2006, 74(21): 214111
29. J. A. Rayne and B. S. Chandrasekhar, Phys. Rev., 1961, 122(6): 1714
30. L. Vitos, Computational Quantum Mechanics for Materials Engineers, London: Springer-Verlag, 2007
31. M. Ropo, K. Kokko, and L. Vitos, Phys. Rev. B, 2008, 77(19): 195445
32. W. B. Pearson, A Handbook of Lattice Spacings and Structures of Metals and Alloys, Belfast: Pergamon, 1958
33. H. L. Zhang, B. Johansson, and L. Vitos, Phys. Rev. B, 2009, 79(22): 224201
34. P. A. Korzhavyi, A. V. Ruban, J. Odqvist, J. O. Nilsson, and B. Johansson, Phys. Rev. B, 2009, 79(5): 054202
35. S. F. Pugh, Philos. Mag., 1954, 45: 823
36. D. G. Pettifor, Mater. Sci. Technol., 1992, 8: 345
37. C. Kittel, Introduction to Solid State Physics, New York: Wiley, 1996
38. A. T. Aldred, Phys. Rev. B, 1976, 14(1): 219
39. C. Paduani and J. C. Krause, Braz. J. Phys., 2006, 36(4a): 1262